***Post-synthetic modification of yttria-stabilized zirconia aerogels with silica coatings for enhanced thermal stability***

Nathaniel S. Olson[1,2†], Jamesa L. Stokes[3†], Haiquan Guo[4], Frances I. Hurwitz[3††], Richard B. Rogers[3], Nachiket Shah[1], Jessica A. Krogstad[1,5*]

[1]*Department of Materials Science and Engineering, University of Illinois Urbana-Champaign, Urbana, IL*

[2]*NASA Johnson Space Center, Houston, TX*

[3]*NASA Glenn Research Center, Cleveland, OH*

[4]*Universities Space Research Association, Cleveland, OH*

[5]*Materials Research Laboratory, University of Illinois Urbana-Champaign, Urbana, IL*

† Authors contributed equally to this work

†† Retired

* Corresponding author (jakrogst@illinois.edu)

**Abstract**

Maintaining high surface area and porosity at high temperatures is important when considering aerogels for use in thermal management systems. The mesoporous structure of aerogels results in extremely low thermal conductivity, making them lightweight, high performance insulating materials. Maintaining these properties requires innovative routes to suppress sintering and pore collapse as use temperatures rise. The current work aims to improve the pore structure stability of yttria-stabilized zirconia aerogels by the addition of a $SiO_2$ coating. The functionalization of surface hydroxyl groups by the addition of $SiO_2$ is hypothesized to mitigate condensation reactions, which are a driving force for shrinkage and pore structure collapse. Zirconia aerogels with 0, 10 and 30 mol% yttria ($YO_{1.5}$) additions were coated in a

tetraethyl orthosilicate (TEOS) solution and exposed to temperatures up to 1200°C. Crystal structure, pore structure, and aerogel morphology were investigated to understand changes in aerogel thermal stability. The $SiO_2$ coating exhibited a greater influence on pore stability over yttria concentration, with specific surface area of the coated aerogels being twice that of the uncoated aerogels up to 1000°C. However, the presence of the $SiO_2$ coating promoted rapid sintering and densification at 1200°C, establishing an upper use temperature for $SiO_2$ and a need to develop other coating chemistries.

**Keywords:** aerogel; zirconia; silica; thermal management; porous ceramics; thermal stability

## 1 Introduction

The highly porous nature of aerogels imparts extraordinary insulative capabilities. The low thermal conductivity is the result of a unique pore structure composed of meso- and small macropores, generally from 10 to 200 nm, preventing heat transfer via conduction and convection. Opacifiers can be added to block radiative transmission if necessary.[1] In high temperature applications where mass is a critical concern, such as spaceflight, aerogels could serve as an exceptional insulator owing to their low thermal conductivity and low density. However, widespread adoption of aerogels for such applications is currently impeded by the rapid densification of the pore structure with increasing temperatures. With such densification, the desirable low thermal conductivity is lost, while simultaneously losing any semblance of structural integrity through shrinkage and cracking.

Adjusting the composition via changing dopants and dopant concentration in zirconia ($ZrO_2$) aerogels led to improvements in thermal stability as detailed in previous work.[2–4] For example, $ZrO_2$ doped with 30 mol% $YO_{1.5}$ (30YSZ) maintained over four times the specific surface area (SSA) at 1000°C compared to undoped $ZrO_2$.[3] Although when the magnitude is considered,

compared to the SSA of 407 $m^2/g$ that 30YSZ started with in the as dried state, only 58 $m^2/g$ remained at 1000°C, a loss of nearly 86%. This reduction is unacceptable in applications with temperatures approaching and exceeding 1000°C. The lessons learned and materials identified in the work on doped zirconia aerogels were informative in selecting baseline materials for further modification towards improved thermal stability.

The high surface hydroxyl content of most metal oxide aerogels provides a vast number of sites for functionalization of the surface. Numerous functional groups and other moieties can be attached to modify the properties and surface chemistry of aerogels, which often proves useful in the field of catalysis.[5–10] Of particular relevance to this work are the capping approach[11] and coating approach[12], both of which have demonstrated improved retention of mesoporosity at elevated temperatures.

For the capping approach, first demonstrated by Wu *et al.*,[11] the surface hydroxyl groups (—OH) of tin(IV) oxide ($SnO_2$), titania ($TiO_2$), and zirconia ($ZrO_2$) aerogels were capped with hexamethyldisilane (HMDS, $[Si(CH_3)_3]_2NH$), forming non-condensable methyl siloxyl groups (—$OSi(CH_3)_3$). The formation of such surface methyl siloxyl groups were postulated to preclude the condensation of surface hydroxyls that would otherwise be a driver of pore collapse. At temperatures exceeding 350°C, the surface groups decompose and were found to redistribute through the intergranular network, presumably as silica particles. This positioning was correlated with reduced grain growth, suggesting that the silica particles were effective grain boundary pinning agents. In this way, the capping approach reduced the two dominant driving forces for densification: surface reconstruction through condensation and crystallite growth, and resulted in a more resilient aerogel structure, at least below 600ºC for the chemistries reported.

The coating approach, on the other hand, involves soaking the gel in a solution containing a metal alkoxide. This could be a solution of tetraethyl orthosilicate (TEOS) in ethanol according to Wang *et al.*[12] or a solution of alkoxide, ethanol, water, and nitric acid according to Zu *et al.*[13] This approach was reported to create a core-shell like structure, once again capable of suppressing the driving forces for structural evolution and densification. Coated $Al_2O_3$, $TiO_2$, and undoped-$ZrO_2$ aerogels did in fact exhibit improved thermal stability, modified phase behavior, and inhibited crystallite growth compared to uncoated materials. The impressive increase in thermal stability and the anomalous crystal structure evolution for coated aerogels warrants further exploration. It is suggested in the work by Zu *et al.*[13] that the formation of silica particles in the intergranular regions within the aerogel ligaments prevents crystallite/grain growth and phase transformation, though the mechanism is not fully understood. The morphology of the $SiO_2$ coating in the work by Zu *et al*. was not clear, but the improvement in thermal stability to 1000°C is remarkable.

In the present work, the coating procedure by Zu *et al*.[13] is adapted for use on YSZ aerogels from 0 to 30 mol% $YO_{1.5}$ with coatings of silica deposited from a TEOS solution. A prodigious leap in thermal stability is conceivable by combining two proven routes to improved thermal stability: doping with yttria and post-synthetic coatings. This work also provides insight to inadequately understood foci, including the structure and chemistry of the coating, the phase and structural evolution of silica coated aerogels beyond 1000°C, and limits of stability for silica coating chemistry. An improved understanding of coated aerogel structure and evolution provided in this work will be an important contribution to the development of a design framework for thermally stable aerogels.

## 2 Experimental procedures

### 2.1 Aerogel synthesis

YSZ aerogels of 0, 10, and 30 mol% $YO_{1.5}$ were prepared using a sol-gel process adapted from previous work.[14] Zirconyl chloride octahydrate ($ZrOCl_2 \cdot 8H_2O$, Alfa Aesar, 99.9%) and yttrium trichloride hexahydrate ($YCl_3 \cdot 6H_2O$, Acros Organics, 99.9%), were first dissolved in 200 proof ethanol (Decon Labs) in separate containers. The standard solids loading was 1.263 mmol metal per mL of ethanol. DI water was added in six times the stoichiometric amount for each metal precursor (e.g. 24 moles water per mole of Zr, 18 moles of water per mole of Y).[15] The precursors were stirred separately for 60 minutes for hydrolysis. The precursors were then combined and stirred for 15 minutes. The solution was placed in an ice bath and propylene oxide (PO) ($CH_3CHCH_2O$, Sigma Aldrich) was added dropwise at a ratio of 2.342 mole PO per mole of metal. The solution was stirred for 5 minutes and then transferred to molds made from polyethylene syringes (24 mL) with the tip cut off. The plunger was placed at 20 mL and the mold was filled to the 10 mL mark. Gelation occurred within 10 to 30 minutes. All gels were held in the mold for 24 hours.

Gels to remain uncoated were extracted into room temperature 200 proof ethanol and aged for 6 days. Gels to be coated with silica were extracted into a coating solution of tetraethyl orthosilicate (TEOS, $Si(OC_2H_5)_4$, Sigma Aldrich, 98%), DI water, and nitric acid ($HNO_3$, Sigma Aldrich 70 wt.%) in 200 proof ethanol and aged for 3 days. The molar ratio of TEOS:ethanol:water:nitric acid was 1:7.7:1.5:0.01, adapted from previous work by Zu *et al.*[13] The coating solutions were stirred for 30 minutes prior to addition of gels. Following 3 days, the coated gels were extracted into 200 proof ethanol and aged for 3 days to remove unreacted TEOS. All gels were supercritically dried using carbon dioxide.[16] The process used four washes in liquid

carbon dioxide to replace ethanol in the pore structure, before bringing the carbon dioxide to its supercritical state and evacuating the fluid.

### 2.2 Heat treatments

For all heat treatments at 600, 1000, and 1200°C, aerogels were placed into high purity alumina crucibles. Heat treatments at 600°C and extended heat treatments above 1200°C were performed in a box furnace under air with a temperature ramp of 20°C/min. For 1000 and 1200°C, the aerogels were heated in a tube furnace under a flowing argon atmosphere and a ramp of 5°C/min. The maximum temperature for the standard 600, 1000, and 1200 °C heat treatments was held for 18 minutes and the aerogels were cooled to room temperature within the furnace.

### 2.3 Material characterization

The as-dried aerogels underwent physical measurement to characterize shrinkage and bulk density. The length and diameter of cylindrical aerogel monoliths were measured and used to calculate bulk density and shrinkage relative to the diameter of the mold. Scanning electron microscopy (SEM) was performed on a Hitachi S4700 or S4800 SEM to characterize pore morphology. Samples were crushed onto carbon tape and imaged uncoated at 2 kV. Energy dispersive spectroscopy (EDS) was performed on a ThermoFisher Axia ChemiSEM. High vacuum mode was used at an accelerating voltage of 30 kV, spot size of 6, and working distance of 10 mm. An area that showed minimal charging was selected and a point analysis (60 s) was run for three points per area. This process was repeated for three areas per sample. The composition was calculated from an average of all point analyses. Samples for (scanning) transmission electron microscopy (S/TEM) were ultrasonicated in ethanol and dispersed on a holey carbon coated copper grid for TEM analysis. Bright field imaging was performed on a JEOL $LaB_6$ TEM and STEM EDS was performed using a FEI Talos STEM (ThermoFisher Scientific).

Nitrogen adsorption/desorption experiments were conducted on Micromeritics ASAP 2020 (NASA Glenn Research Center) and Micromeritics 3Flex (University of Illinois at Urbana-Champaign, School of Chemical Sciences, Microanalysis Laboratory) to measure the specific surface area via the method of Brunauer-Emmett-Teller (BET) and porosity via the method of Barret-Joyner-Halenda (BJH). Average pore size and cumulative pore volume were calculated using the BJH desorption method. Prior to adsorption/desorption, samples were degassed under vacuum and heated at 5°C/min to 80°C with an 8 hour hold.

Powder X-ray diffraction (XRD) was used to identify the crystalline phase and calculate the crystallite size via the Scherrer equation. To prepare samples for XRD, powders were crushed in a mortar and pestle with a small amount of isopropanol. The suspension was dropped via pipette onto a low background holder. XRD was performed on a Bruker D8 Advance (Cu Kα, 1.5406Å) from 10 to 100° 2θ, 0.02° per step, and 0.25 seconds per step. Quantitative phase analysis (QPA) was performed using whole pattern fitting (WPF, also known as Rietveld refinement) with pseudo-Voigt fits as implemented in the JADE (Materials Data, Inc.) analysis program with the International Center for Diffraction Data (ICDD) crystallographic database. The following powder diffraction files (PDF) were used: zirconium oxide, monoclinic (04-004-4339), zirconium oxide, tetragonal (04-005-4207), zirconium oxide, cubic (04-002-8314), and cristobalite (04-007-2134).

## 3 Results

### 3.1 As-dried aerogel structure

Table 1 summarizes the physical and textural properties of the as-dried (AD) aerogels following supercritical drying. Comparing the uncoated samples, specific surface area (SSA) was highest for 0YSZ and lowest for 10YSZ. Pore volume and average pore size increased with increased yttria content. Both shrinkage and bulk density were reduced with increased yttria

content. The effects of $SiO_2$ coating on the properties of the AD aerogel were generally dependent on the yttria content. For all three compositions, the coating reduced the shrinkage, with the effect most pronounced for 0YSZ. The bulk density was reduced for $SiO_2$-0YSZ but increased for $SiO_2$-10YSZ and $SiO_2$-30YSZ. The coating modestly increased the SSA for 0YSZ and strongly increased the SSA for 30YSZ, with a slight reduction in SSA for 10YSZ. Pore volume and pore size for 0YSZ were nearly doubled upon coating and the increases in pore volume and size were modest for 10YSZ. 30YSZ pore volume and pore size were reduced slightly upon coating. The AD pore size distributions revealed a broadening in the distribution for all materials upon coating. Qualitatively, coated aerogels were much more robust during handling.

The amount of Si deposited on the aerogel was quantified with EDS for 30YSZ. Attempts to use ICP-OES were unsuccessful in quantifying the silicon content accurately. The average atomic ratio of Zr:Y:Si in 30YSZ-$SiO_2$ was 1.00:0.55:3.01 with no discernable dependence of composition on location. EDS mapping did not reveal any inhomogeneities in the composition of the coated aerogel, though the resolution of the instrument was likely not adequate in this regard.

**Table 1.** The physical and textural properties of as dried (AD) aerogels following supercritical drying. Increased yttria content coarsens the pore structure. Generally, the effects of coating are dependent on the yttria content, but shrinkage is reduced for all materials following coating.

| Sample | SSA ($m^2/g$) | $V_{BJH}$ ($cm^3/g$) | $D_{BJH}$ (nm) | S (%) | $\rho_b$ ($g/cm^3$) |
|---|---|---|---|---|---|
| 0YSZ | 504 | 1.291 | 7.0 | 29.5 | 0.292 |
| $SiO_2$-0YSZ | 518 | 2.267 | 13.9 | 15.8 | 0.230 |
| 10YSZ | 455 | 1.793 | 12.3 | 20.7 | 0.198 |
| $SiO_2$-10YSZ | 448 | 1.892 | 15.9 | 14.1 | 0.227 |
| 30YSZ | 473 | 2.914 | 26.9 | 12.5 | 0.186 |
| $SiO_2$-30YSZ | 599 | 2.843 | 25.1 | 10.7 | 0.275 |

SSA = BET specific surface area
$V_{BJH}$ = BJH desorption cumulative pore volume
$D_{BJH}$ = BJH desorption average pore diameter
S = as dried shrinkage (diameter)
$\rho_b$ = bulk density

### 3.2 Aerogel morphology and thermal stability

Nitrogen physisorption quantified the SSA, pore volume, and pore size for the as dried (AD) material and following heat treatments at 600, 1000, or 1200°C as shown in Figure 1. At 600°C, all three coated materials maintained significantly more SSA than their uncoated counterparts, ranging from a factor of 2.3 increase in SSA for 30YSZ and a factor of 7.3 increase for 0YSZ, depicted in Figure 1(a). Among the uncoated materials, increased yttria content led to an increase in SSA at 600, 1000, and 1200°C consistent with previous results for YSZ.[2–4] This trend was not replicated for the coated materials. At 600°C, $SiO_2$-0YSZ maintained the highest SSA with 494 $m^2/g$. $SiO_2$-10YSZ and $SiO_2$-30YSZ were found to have identical SSAs of 378 $m^2/g$. At 1000°C, $SiO_2$-0YSZ and $SiO_2$-10YSZ had virtually identical SSAs (226 and 223 $m^2/g$, respectively). At 1200°C, SSA was unmeasurable for coated and uncoated 0YSZ and 10YSZ. Both coated and uncoated 30YSZ samples maintained some SSA to 1200°C, with 16 $m^2/g$ for uncoated and 21 $m^2/g$ for coated. Similar results were obtained for the pore volume to 1000°C in Figure 1(b), where coated materials maintained greater pore volume than all uncoated materials.

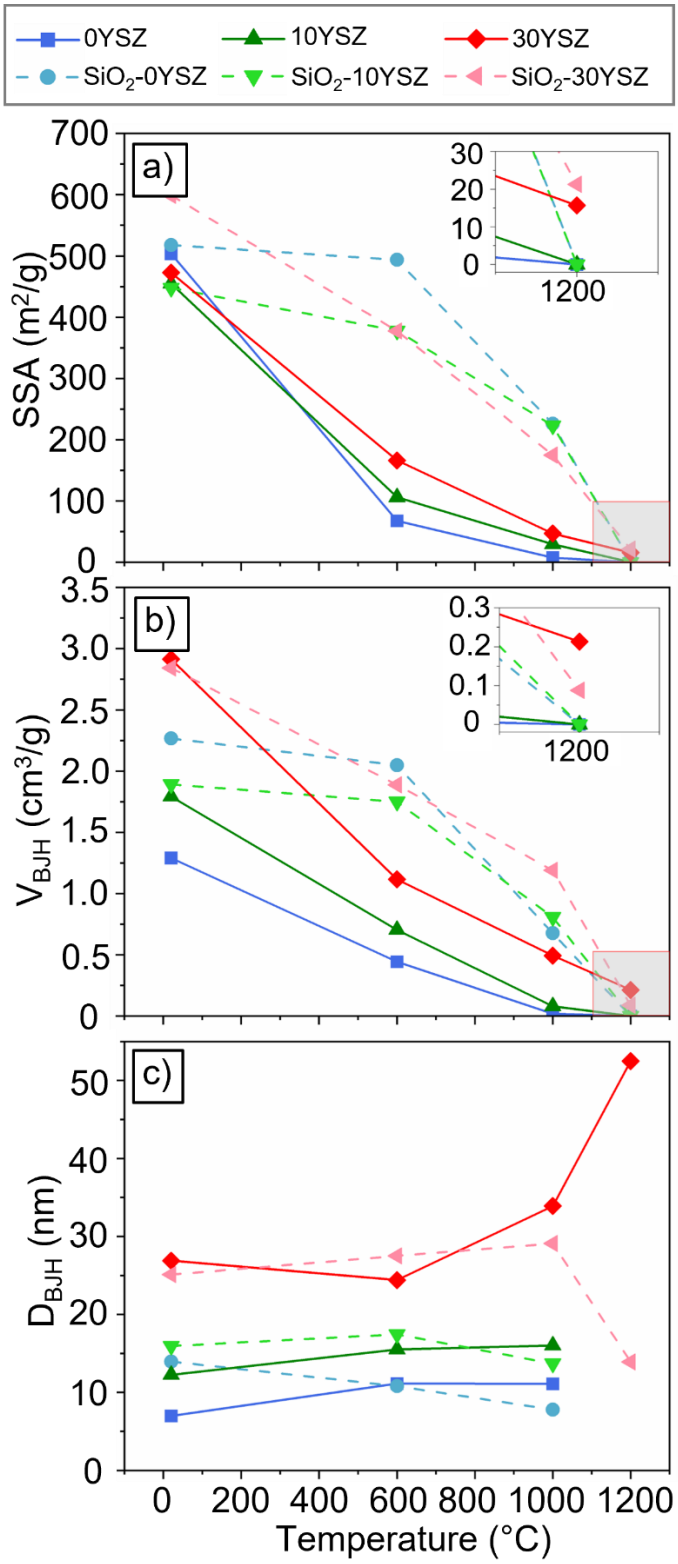


**Figure 1.** a) BET specific surface area, b) desorption cumulative pore volume, and c) desorption average pore size for aerogels as a function of temperature. The dark solid lines are uncoated and light dashed lines are coated.

Again, increased yttria content increased pore volume at all temperatures for uncoated materials. At 1000°C, $SiO_2$-30YSZ maintains the greatest pore volume with 1.190 $cm^3/g$. At 1200°C, pore volume was unmeasurable for coated and uncoated 0YSZ and 10YSZ. Uncoated 30YSZ had the highest pore volume at 1200°C with 0.213 $cm^3/g$. As shown in Figure 1(c), pore size increased with increased yttria content as described previously. To 1000 °C, pore size remained relatively constant for all materials with no clear impact from coating. From 1000 to 1200°C, the pore size increased from 33.9 to 52.5 nm for uncoated 30YSZ and decreased from 29.1 to 13.9 nm for $SiO_2$-30YSZ. Pore size could not be analyzed for coated and uncoated 0YSZ and 10YSZ heat treated to 1200ºC on account of no measurable surface area or mesoporosity.

The BJH desorption pore size distributions are included in Figure 2. From AD to 600°C, the pore size distribution changes significantly for all materials with the exception of uncoated 10YSZ, $SiO_2$-10YSZ, and $SiO_2$-30YSZ. By 1000°C, the pore size distribution is essentially flat for uncoated 0YSZ and hardly detectable for uncoated 10YSZ. For the coated materials from 600 to 1000°C, the distribution shifts to smaller average pore size for $SiO_2$-0YSZ and $SiO_2$-10YSZ, though the effect is most pronounced for $SiO_2$-0YSZ. The distribution for $SiO_2$-30YSZ is remarkably stable from AD to 1000°C, with only a slight reduction in volume from larger pores. At 1200°C, coated and uncoated 0YSZ and 10YSZ have no measurable pore size distributions as described above. For 30YSZ, the change in distribution for the coated material is drastic, with only a minor amount of smaller pores, most less than 20 nm, remaining in the material. The uncoated 30YSZ also loses much of its pore volume at 1200°C, but without the significant shift in the average pore size.

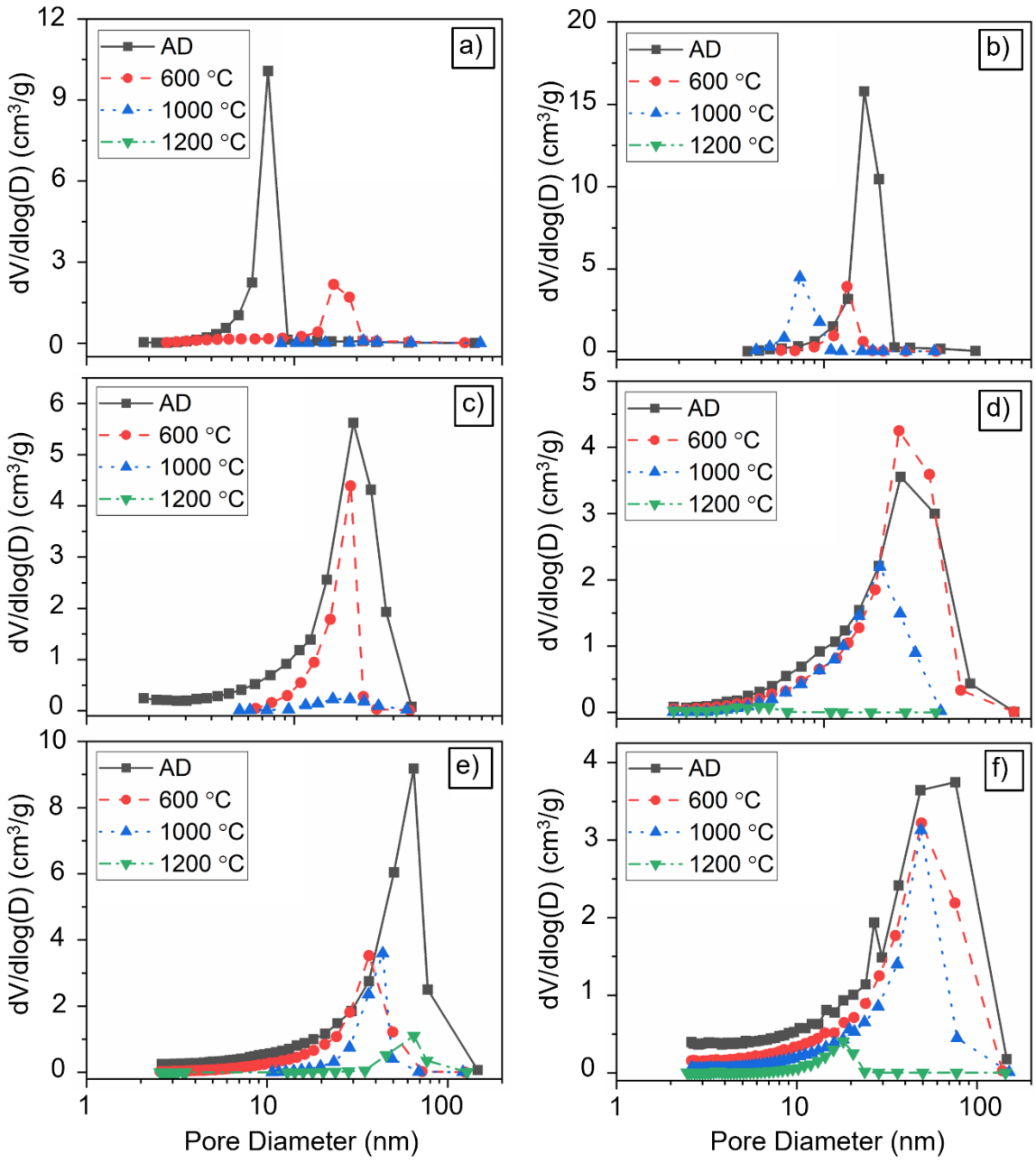


**Figure 2.** Pore size distributions for a) 0YSZ, b) $SiO_2$-0YSZ, c) 10YSZ, d) $SiO_2$-10YSZ, e) 30YSZ, and f) $SiO_2$-30YSZ.

SEM micrographs of the aerogels are displayed in Figure 3. From AD to 1000°C, there were no discernable differences at the resolution available with SEM between the coated and uncoated samples, with the notable exception of 0YSZ at 1000°C. For uncoated 0YSZ at 1000°C, spherical

particles with some apparent necking between particles were observed. Distinct particles were no longer evident for uncoated 0YSZ at 1200°C, and the sample morphology resembled fully densified material with grains around ~1 μm in size. No comparable particles or grains were observed in $SiO_2$-0YSZ at 1000°C or 1200°C.

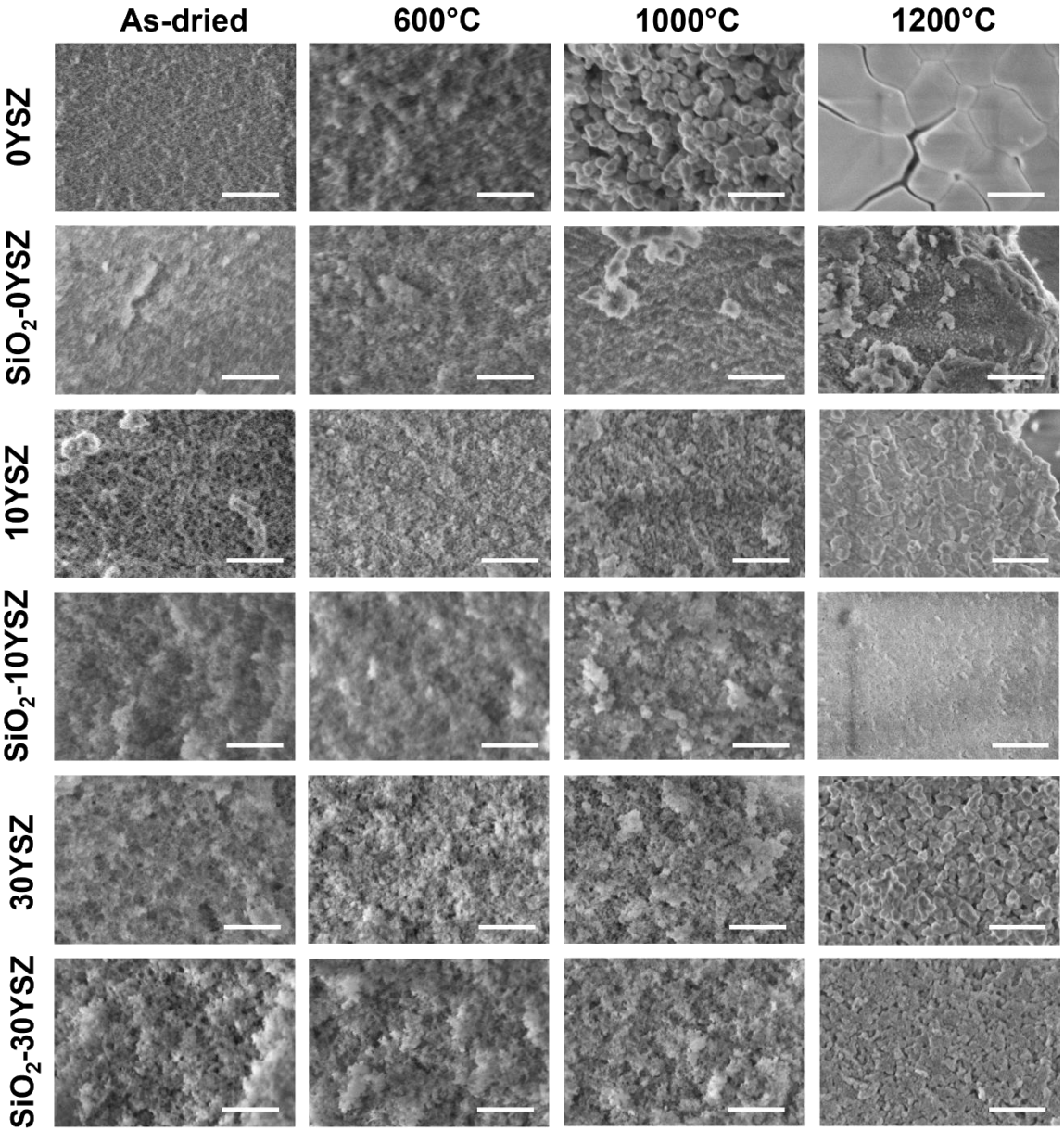


**Figure 3.** SEM micrographs of uncoated and coated 0YSZ, 10YSZ, as 30YSZ, aerogels as dried, after 600°C, after 1000°C, and after 1200°C. The scale bar in all images is 500 nm.

At 1200°C, 10YSZ and 30YSZ, both coated and uncoated, showed distinct evolution in morphology. 10YSZ and 30YSZ showed significant particle growth and necking between particles. The sponge-like mesoporous network was no longer visible, replaced by large macropores between partially sintered particles. The changes in morphology of $SiO_2$-10YSZ and $SiO_2$-30YSZ were even more dramatic. Not only did it appear as if particles had grown but also sintered together to a greater extent than in the uncoated samples. The macropore size in the coated samples are clearly smaller than that in the uncoated samples. This result harkens to the change in average mesopore size from 1000 to 1200°C shown in Figure 1(c), where 30YSZ increased and $SiO_2$-30YSZ decreased in average pore size.

Given the limits of resolution with SEM, TEM was also performed on $SiO_2$-30YSZ heat treated at 1000 and 1200°C and the images are shown in Figure 4(a) and 4(b), respectively. At 1000°C, the small particle size and mesoporosity was visible. The morphology changed significantly after heat treatment at 1200°C. The particle size was significantly larger than at 1000°C. Furthermore, mesoporosity was no longer visible. The sample took on the appearance of well-defined spherical particles embedded in a continuous matrix. From the TEM images, the line-intercept method was employed to estimate particle size. At 1000°C, the estimated particle size was 5.2 (±0.7) nm. At 1200°C, the estimated particle size was 16.0 (±1.7) nm.

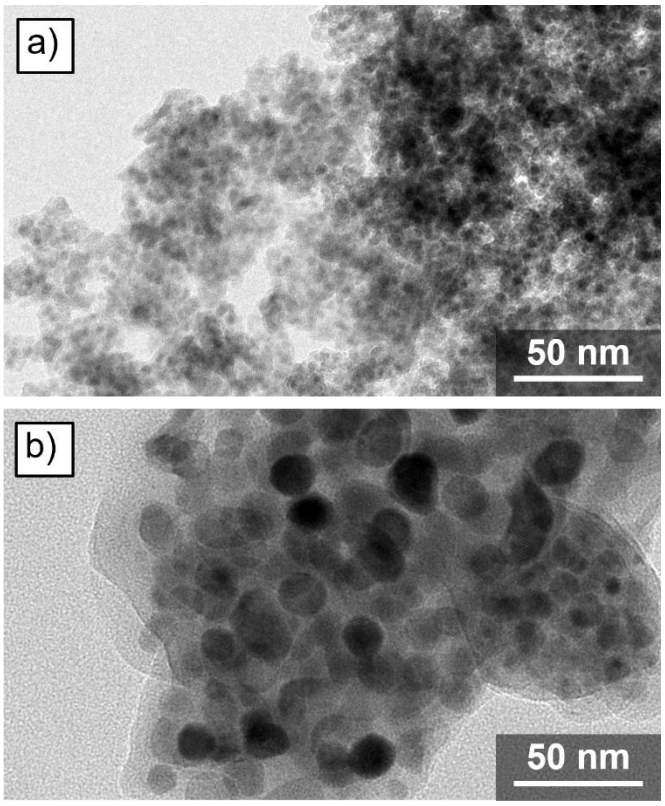


**Figure 4.** Bright field TEM comparison of $SiO_2$-30YSZ at (a) 1000°C and (b) 1200°C. From 1000 to 1200°C, significant particle growth and densification is observed.

### 3.3 Crystal structure evolution

All aerogel samples were X-ray amorphous after supercritical drying. The XRD data for the heat-treated uncoated 0YSZ, 10YSZ, and 30YSZ samples are displayed in Figure 5. The XRD data for all coated aerogel samples are displayed in Figure 6. In uncoated 0YSZ (Figure 5(a)), heat treatment at 600°C resulted in crystallization of the aerogel to a mixture of monoclinic $ZrO_2$, along with a tetragonal $ZrO_2$ phase that is presumably restricted from full transformation to the monoclinic phase due to the fine crystallite size at this point.[17, 18] With an increase in heat treatment temperature to 1000°C and 1200ºC, monoclinic $ZrO_2$ became the dominant phase observed in the XRD data. At 1000°C, a small peak around ~30° 2θ was attributed to the minor presence of tetragonal $ZrO_2$, although this phase was no longer observable at 1200°C.

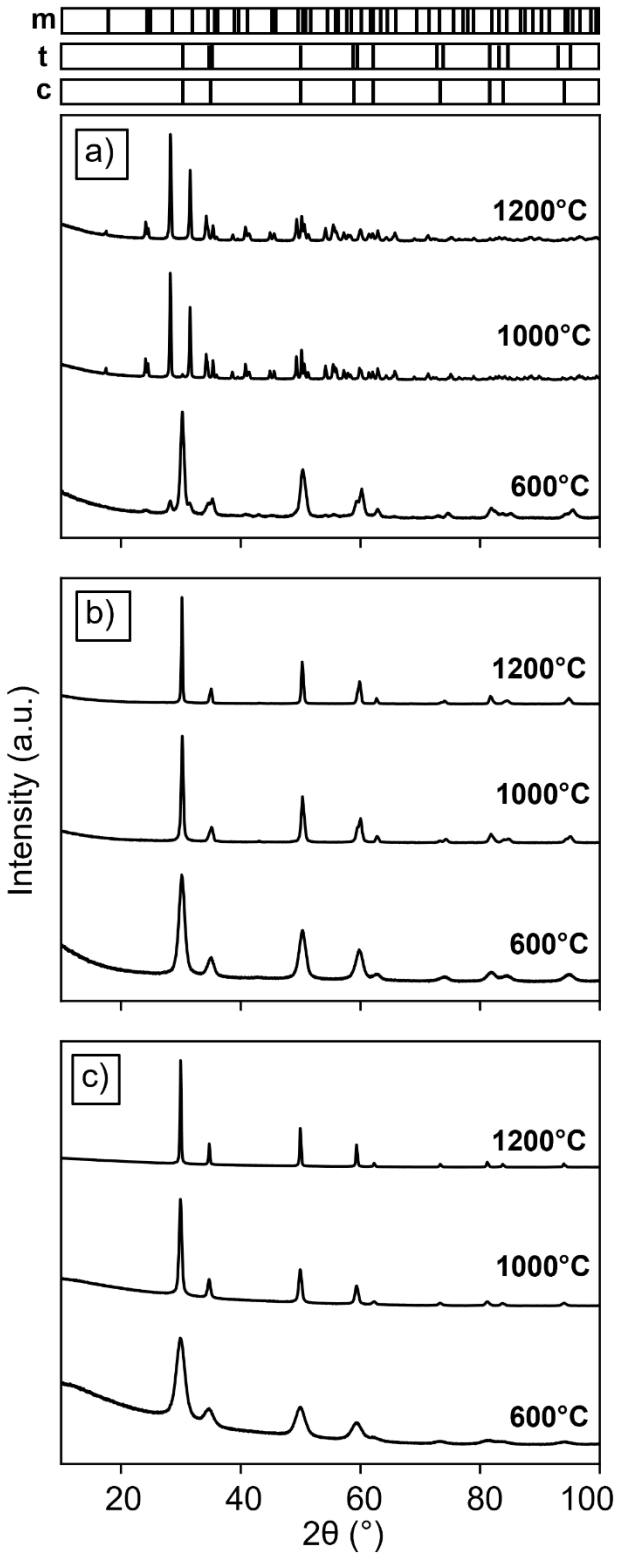


**Figure 5.** XRD scans of heat-treated aerogels a) 0YSZ b) 10YSZ, and c) 30YSZ.

With increasing temperature, the peak shapes qualitatively tended to decrease in width and increase in intensity. Such a trend could be indicative of increasing crystallite size and/or crystalline content. In the $SiO_2$-0YSZ samples (Figure 6(a)), no distinct crystallization was observed in the samples heat treated at 600°C. Heat treatment at 1000°C resulted in the formation of very wide but distinct tetragonal/cubic phase peaks. These peaks narrow after heat treatment at 1200°C, similar to uncoated 0YSZ in Figure 5(a). While the monoclinic phase was the dominant phase at 1200°C in uncoated 0YSZ, monoclinic $ZrO_2$ was only observed as a minor phase in $SiO_2$-0YSZ at 1200°C (Figure 6(a)).

Regardless of the heat treatment temperature, 10YSZ samples did not present any evidence of phase transformation to a monoclinic phase upon crystallization and cooling. Given the fine crystallite size, a more robust distinction between potentially present cubic or tetragonal phases was not possible. In uncoated 10YSZ (Figure 5(b)), heat treatment at 600°C resulted in crystallization of the aerogel, similar to uncoated 0YSZ. With increasing temperature, these peaks became narrower and increased in magnitude. XRD analysis of $SiO_2$-10YSZ (Figure 6(b)) showed little to no evidence of crystallization at 600°C, correlating well with the results obtained on $SiO_2$-0YSZ. Up to 1200°C, the peak widths of the coated samples were consistently wider than the uncoated samples for 10YSZ. In $SiO_2$-10YSZ, there was also a small amorphous hump (highlighted by black arrow in figure) present at low angles, being most distinct at 1200°C.

The 30YSZ sample exhibited crystallization to the cubic phase at 600°C (Figure 5(c)), which persisted in additional heat treatments at both 1000°C and 1200°C. Though the tetragonal phase cannot be ruled out from the XRD patterns, consideration of the yttria doping level and the pattern together supports formation of the cubic phase. No evidence of crystallization of $SiO_2$-30YSZ was observed at 600°C. The formation of very minor peaks were observed after heat treatment of $SiO_2$-

30YSZ at 1000°C, although the sample appeared to remain largely amorphous. At 1200°C, distinct cubic peaks were formed in $SiO_2$-30YSZ.

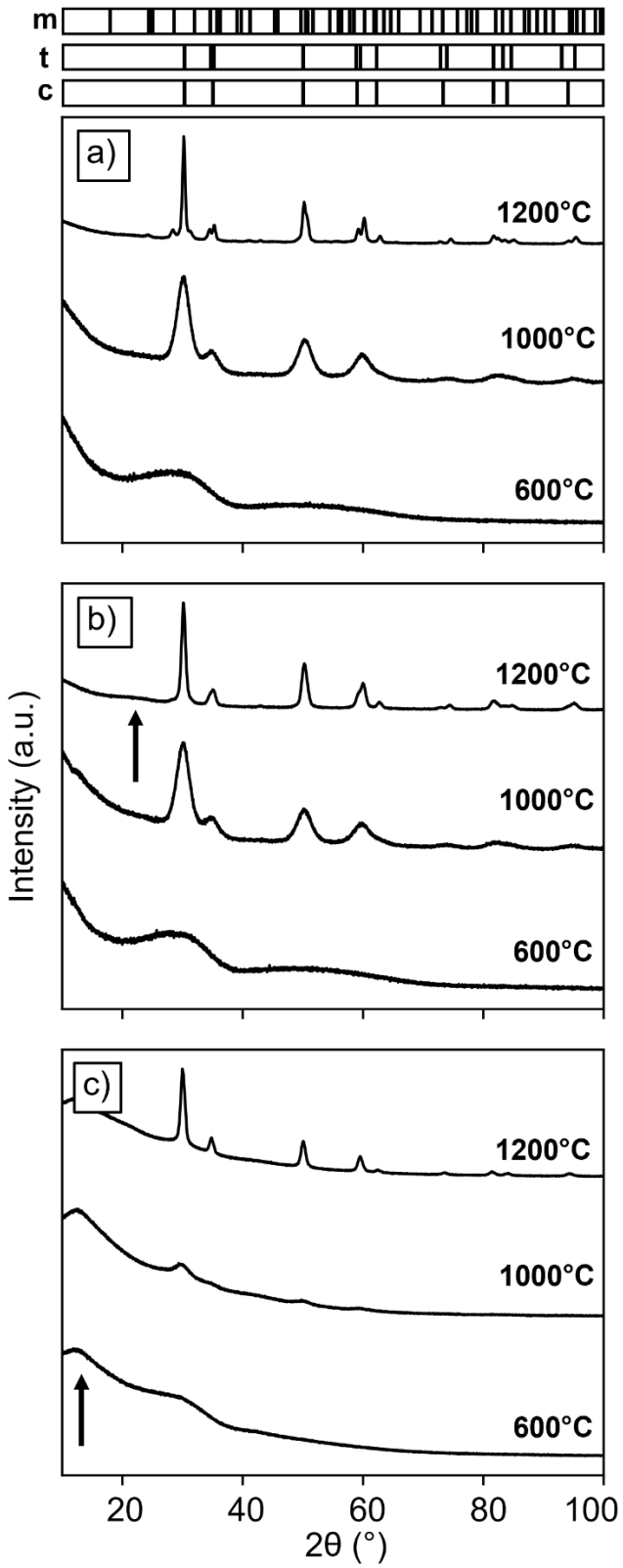


**Figure 6.** XRD scans of heat-treated aerogels a) $SiO_2$-0YSZ b) $SiO_2$-10YSZ, and c) $SiO_2$-30YSZ. Arrows point towards broad peaks attributed to an amorphous phase.

A similar amorphous hump (highlighted by black arrows in Figures 5 and Figure 6) with slighter greater magnitude was also observed in $SiO_2$-30YSZ (Figure 6(c)) and was consistently observed from 600°C to 1200°C. This amorphous hump was not observed in uncoated 30YSZ, suggesting that the $SiO_2$ coating may be contributing to the formation of a separate amorphous phase after heat treatment. This is consistent with the TEM observations presented in Figure 4(b).

More thorough interrogation of the crystallinity, morphology, and chemical distribution in the $SiO_2$-30YSZ sample was carried out via STEM, displayed in Figure 7. Bright field micrographs (Figure 7(a) showed globular, crystalline particles interspersed in an apparently non-crystalline phase, per the absence of any discernable lattice fringes. EDS compositional analysis (Figure 7(c)) carried out in dark field (Figure 7(b)) indicated that the bright globular particles were rich in both Zr and Y, while the surrounding areas were rich in Si, confirming that the $SiO_2$ coating was, at least partially, segregated into a distinct and separate phase from 30YSZ after this heat treatment.

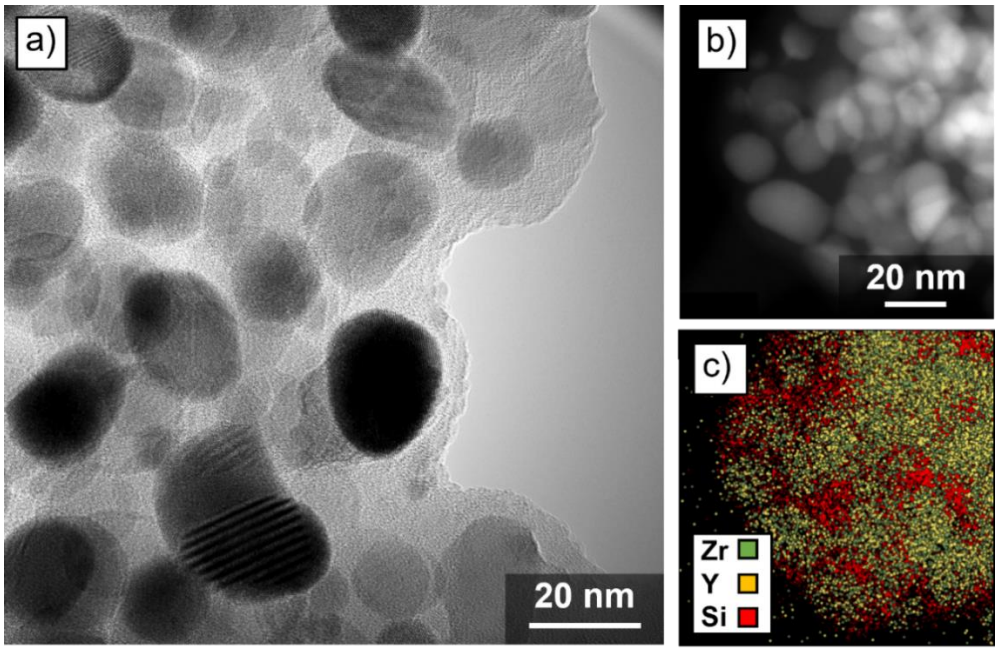


**Figure 7.** a) Bright field and b) HAADF STEM micrographs of $SiO_2$-30YSZ heat treated at 1200°C and c) EDS compositional map of b).

Given the observed difference in crystallization behavior, the emergence of a potentially amorphous secondary matrix phase and qualitative peak sharpening trends, a more comprehensive analysis of crystallite size evolution was merited beyond what was possible to observe via S/TEM on the $SiO_2$-30YSZ specimens (Figures 4 and 7). A modified Scherr analysis (Figure 8) was performed on the Gaussian fitted peak shapes as a route to document *relative* changes in crystallite size between compositions and coating conditions. The modification involved dividing the crystallite size, D, by the dimensionless shape factor, C, to allow for relative comparison of crystallite sizes among samples. The absolute crystallite size is more directly extracted from the TEM observations that have already been presented, but this level of analysis was not possible for all specimens. Little to no crystallization of any of the coated samples was observed at 600°C, so crystallite size could not be quantified at this temperature. In both the undoped and the 10YSZ samples, it was apparent that the coated samples consisted of crystallites at least an order of magnitude smaller in size than the uncoated samples at 1000°C, while little to no crystallization had begun at 1000ºC for the $SiO_2$-30YSZ sample. There was not a large difference in crystallite size between the 10YSZ and 30YSZ samples at 1000°C. It appeared that at this temperature, the $SiO_2$ coating exhibited a greater influence on the size of the crystallites than the dopant concentration. At 1200°C, the crystallite size of $SiO_2$-10YSZ and $SiO_2$-30YSZ were comparable, and just smaller than $SiO_2$-0YSZ.

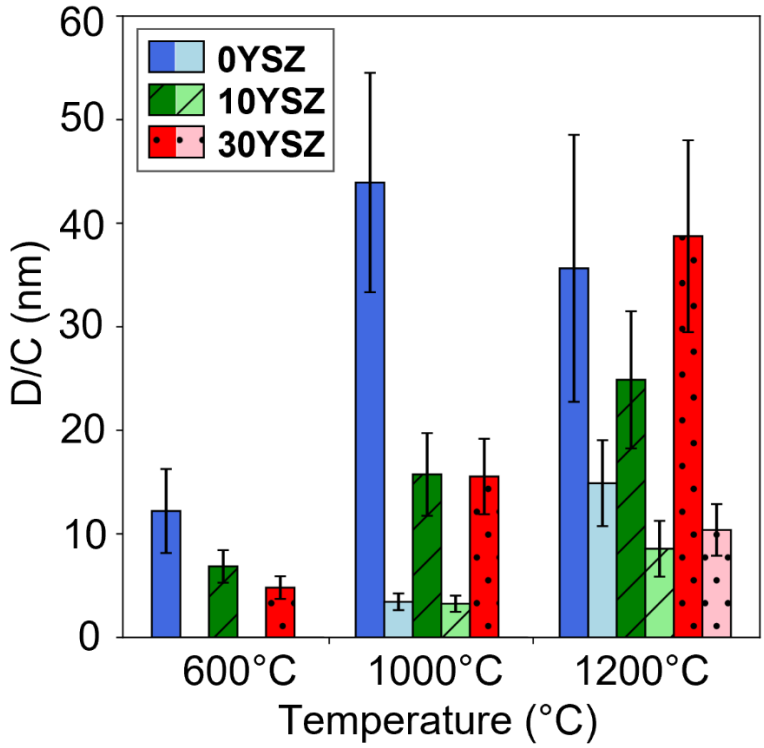


**Figure 8.** Normalized crystallite sizes of uncoated (darker bars) and coated (lighter bars) 0YSZ, 10YSZ, and 30YSZ aerogels after heat treatment. The sizes, D, are normalized by the dimensionless shape factor, C.

The confluence of XRD and S/TEM data presented thus far suggests the eventual segregation of a distinct, amorphous Si-rich phase. Additional heat treatments were therefore carried out to assess the bounds of this behavior for the $SiO_2$-30YSZ aerogels. The XRD data collected following these heat treatments are plotted in Figure 9. The original $SiO_2$-30YSZ sample heat treated at 1200°C is included in the figure for comparison. As previously stated, there was a large amorphous hump present in this sample at low angles after the initial heat treatment at 1200°C. This amorphous signal decreased in intensity upon further heat treatment at 1200°C for 12 hours, and no additional phases were observed. Heat treatment at 1400°C for 12 hours resulted in the crystallization of α-cristobalite, a low temperature tetragonal polymorph of $SiO_2$.

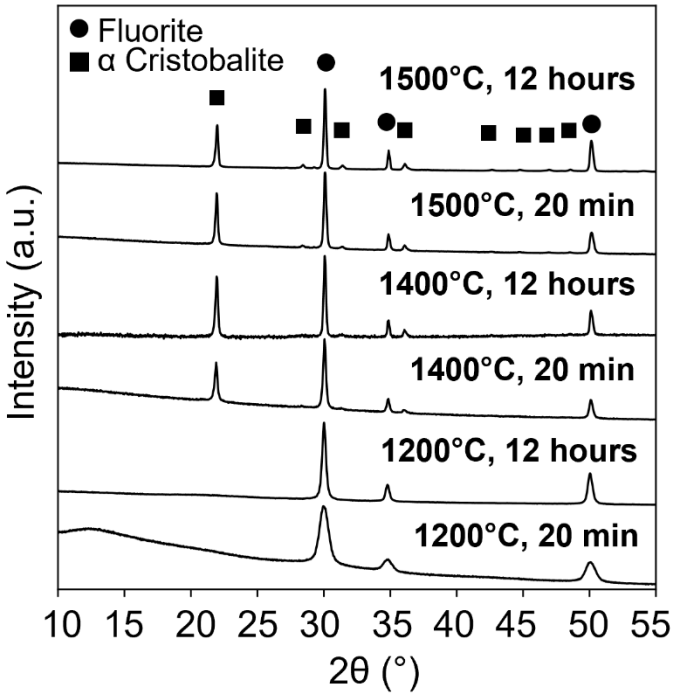


**Figure 9.** XRD of heat-treated $SiO_2$-30YSZ aerogels with reference markers for the cubic phase (●, fluorite) and α-cristobalite phase (■).

The crystallization of cristobalite was also observed at 1500°C after 20 min and at 1500°C after 12 hours. The reduction in magnitude of the amorphous hump after 12 hours at 1200°C (and the subsequent crystallization of $SiO_2$ at higher temperatures) suggested that the onset of devitrification may have been possible at this temperature but remained undetectable via XRD.

## 4 Discussion

Given the exciting stability of silica coated YSZ aerogels presented above, it is valuable to consider possible mechanisms responsible for the initial changes in the as-dried structure, the unique evolution of the coated aerogels and the eventual thermal stability or lack thereof above a critical temperature. The following discussion will address each of these points in greater depth.

### 4.1 Changes to the as-dried structure upon coating

The effect of yttria content on the as dried structure has been established previously.[2–4] Increased yttria content forms a coarser structure, with lower SSA and larger pore size. These trends were observed in this work, with the pore size increasing from 0 to 30 mol% $YO_{1.5}$ for both coated and uncoated aerogels. These changes to the as dried structure have been previously attributed to a change in the average precursor oxidation state[4].

The effects of coating on the structure can be inferred from the physical measurements of the aerogel, including shrinkage and density, and the measurements of the mesoporous structure with nitrogen physisorption. For all compositions, addition of the coating reduced the shrinkage. The reduction in shrinkage is likely a result of increased robustness of the gel towards the pressures that drive shrinkage during gelation and drying. The difference in shrinkage between coated and uncoated was reduced with increased yttria content. This change could simply be related to the propensity of the uncoated gel to shrink, perhaps related to a weaker gel structure. With a stronger gel, the amount of shrinkage is reduced and the effect of coating on reducing shrinkage is not as evident.

The change in density is likely a convolution of change in shrinkage and material deposition from the coating process. For a fixed shrinkage, and therefore gel size, coating will deposit material on the gel and lead to an increase in density. A reduction in shrinkage, all other factors equal, would typically reduce the density of an aerogel since a given mass of solution-phase precursors occupies a greater volume in the gel form. For 0YSZ, the shrinkage is dramatically reduced from 29.5 to 15.8%. The reduction in shrinkage appears to outweigh the effect of material deposition, and the bulk density for this material decreased. For 10 and 30YSZ, the change in shrinkage was smaller, and the deposition of material led to an increase in bulk

density. Though an increase in density is not necessarily ideal for the purposes of lightweight insulation, the potential for an improvement in thermal stability at temperatures of interest may well be worth the cost.

When interpreting the results of nitrogen physisorption, it is essential to keep in mind the limitations of the technique. Adsorption can occur on any free surface that is accessible to nitrogen molecules so calculation of SSA includes both mesoporosity (2 to 100 nm) and macroporosity (> 100 nm). The BJH method for calculating cumulative pore volume, average pore size, and pore size distribution relies on the phenomenon of capillary condensation, which occurs over the mesopore range (2 to 100 nm) and up to 150 nm. Therefore, the cumulative pore volume and average pore size only represent mesopores and not macropores. With this limitation of nitrogen physisorption in mind, for 30YSZ, the slight reduction in mesopore volume and size likely reflects the filling of some mesoporosity with reacted TEOS. Since the change in mesopore volume and size is small in relation to the change in SSA, the significant increase of SSA is likely the result of increased macroporosity, which itself stems from reduced macroscopic shrinkage of the aerogel. Though the pore size distributions in Figure 2 cannot directly measure macroporosity larger than 150 nm, a possible change in macroporosity can still be gleaned when comparing the AD distributions in Figure 2(e) or 30YSZ and Figure 2(f) for $SiO_2$-30YSZ. The distribution for xYSZ-$SiO_2$ indicates greater pore volume contributions from pores of 100 to 150 nm compared to xYSZ for x = 0, 10, and 30. A shift towards larger mesopore sizes is also reported for coated aerogels by Zu *et al*.[13] This shift, along with the reduction in macroscopic shrinkage and small change in mesopore volume, suggests that increased macroporosity is the source of increased SSA in $SiO_2$-30YSZ. The modest increase in pore volume and pore size in 0 and 10YSZ may be the result of the greater reduction in shrinkage for these materials.

### 4.2 $SiO_2$ coating evolution

The addition of a $SiO_2$ coating appeared to suppress and/or delay crystallization and densification of the aerogels up to 1000°C. In the coated samples, there was also an amorphous hump present at low angles (more apparent in the coated 30YSZ samples (Figure 6(c)), and no $SiO_2$-containing crystalline phases (such as crystalline $SiO_2$, zircon [$ZrSiO_4$], or yttrialite/yttrium disilicate [$Y_2Si_2O_7$]) were observed. These results indicated that $SiO_2$ may be present as an amorphous coating on the $ZrO_2$ aerogel up to 1200°C, exhibiting limited reactivity with the aerogel itself. According to thermodynamic assessment of the $ZrO_2$-$SiO_2$ binary system [19–21], $SiO_2$ has no solid solubility in any polymorph of $ZrO_2$ and vice versa. Additionally, $ZrSiO_4$ should be present in mixtures of $ZrO_2$ and $SiO_2$ up to ~1700°C. However, the current results suggest that the amorphous $SiO_2$ coating is not reacting with $ZrO_2$ or $Y_2O_3$ to form any extraneous phases, and the $SiO_2$ itself is not crystallizing at temperatures up to 1200°C despite thermodynamic prediction from binary studies of the $ZrO_2$-$SiO_2$ system. It is important to note that $SiO_2$ was added as a coating only after the precursors for 30YSZ were mixed and a gel was formed. The separate addition of $SiO_2$ to the coated gels could have contributed to the lack of reaction with 30YSZ to form $SiO_2$-containing phases, given that it was not directly mixed into the gel with $ZrO_2$ and $Y_2O_3$ precursors. Additionally, no stable ternary compound exists in the $ZrO_2$-$Y_2O_3$-$SiO_2$ system, although an invariant reaction of c-$Zr_{0.8}Y_{0.2}O_{1.9}$+$SiO_2$→0.8$ZrSiO_4$+0.1$Y_2Si_2O_7$ was reported to occur when the system was assessed at 1400°C and 1600°C.[20]

The devitrification of $SiO_2$ has been shown to be driven by nucleation (rearrangement of atoms) and diffusion (crystallite growth).[22–24] Higher temperatures tend to decrease the incubation period for nucleation, leading to faster crystallization. For pure fused $SiO_2$, the onset of devitrification typically occurs at minimum ~1300°C, although the presence of impurities or

network modifiers (e.g. borosilicate glasses) can decrease this temperature as well as increase the kinetics of crystallization.[25–27] At 1200°C, 12 hours, nucleation of cristobalite possibly occurred in $SiO_2$-30YSZ (which may explain the decrease in magnitude of the amorphous hump, as shown in Figure 9), but the temperature was too low to drive diffusion of nuclei to promote crystallite growth. Additionally, because $SiO_2$ was not directly mixed with $ZrO_2$ or $Y_2O_3$ precursors, the limited presence of network modifiers in the amorphous $SiO_2$ phase is consistent with the observed retardation of crystallization.

### 4.3 Thermal stability of coated aerogels

Coated aerogels displayed significantly higher thermal stability at 600 and 1000°C, exhibiting far less dramatic reductions in SSA and $V_{BJH}$ when compared to uncoated aerogels after the same heat treatments. Taking 30YSZ as an example, the improvement upon coating at 600°C was 2.3 times the SSA and 1.7 times the $V_{BJH}$ relative to the uncoated 30YSZ. This improvement in performance with coating grew at 1000 °C, at which point $SiO_2$-30YSZ maintained 3.7 times the SSA and 2.4 times the $V_{BJH}$ of 30YSZ. This divergence in performance is visually indicated in Figure 1(a-b).

As shown previously, increasing the concentration of $YO_{1.5}$ in a $ZrO_2$ aerogel increased the SSA at 1000°C by a factor of 4.8, relative to an undoped $ZrO_2$ aerogel.[3] This improvement was built upon by coating 30YSZ with $SiO_2$, wherein the SSA at 1000°C increased by a further factor of 3.7 relative to 30YSZ. The improvement achieved in 30YSZ with $SiO_2$ coating can be compared to previous capped and coated aerogels. In the work by Wu *et al*., $SnO_2$ aerogels capped with HMDS maintained 3 times the SSA at 600°C.[28] Without the HMDS treatment, the $SnO_2$ aerogel's SSA was more than halved by 400 °C, whereas the capped aerogel increased in SSA to this temperature. The $ZrO_2$ aerogels with $ZrO_2$/$ZrO_2$-$SiO_2$/$SiO_2$ coatings in work by Zu *et al*. had 2.4

times the SSA at 600°C and 4 times the SSA at 1000°C compared to their uncoated counterparts.[13] These values are closely in agreement with the improvements achieved in this work, though the present study offers the ability to further probe the source of thermal stability in silica coated aerogels.

This improvement in thermal stability is meaningful in the context of applications that require highly insulative mesoporous materials exposed to temperatures up to 1000°C. To expand the impact of this improvement, a deeper understanding of the source of thermal stability for coated aerogels will prove useful in developing refined coating approaches that enhance thermal stability to an even greater degree than achieved here. To this end, several sources and mechanisms of improved thermal stability must be evaluated. Several mechanisms have already been posited and these will be reviewed in the context of another potentially critical driving force, specific surface energy, that is highlighted by the data presented here.

The work by Zu and Wu both tout the effect of surface $SiO_2$ particles to pin grain and particle boundaries, inhibiting both densification and crystallite and/or grain growth.[13, 28] Formation of secondary phases and/or particles at interfaces has repeatedly been demonstrated to induce solute drag and inhibit particle, grain, and crystallite growth.[29–39] The inhibition of growth is generally achieved with small amounts of the secondary phase, often less than 10 mol%, and is the result of space charge effect, reduction in surface energy with an increase in the surface excess of the dopant, or a shift in the relative values of surface and grain boundary energies.[29, 32] On the other hand, $SiO_2$ has also been employed as a sintering aid for ceramics, especially in cases where the concentration of $SiO_2$ is high, allowing the $SiO_2$ to form a continuous film and enable liquid phase sintering.[40, 41] The pitfall of viscous sintering, which is particularly relevant given the high concentration of Si measured in the coated YSZ aerogels, will be further discussed in the next

section. Given the 3:1 ratio of Si to Zr measured in the coated aerogel, referring to the $SiO_2$ phase as a secondary phase or pinning phase may not be accurate. The present work also suggests that some combination of these opposing effects (suppressed grain growth vs. enhanced sintering) may coexist in the present specimens. Notably, coating with silica pushes the onset of crystallization in the aerogels to much higher temperatures than uncoated specimens. But once these crystallites are formed, the presence of silica not only continued to suppress crystallite growth from 1000 to 1200°C, but also contributed to significant densification over this same temperature range.

Beyond solute drag and viscous sintering, particle size has been suggested to also play a role in aerogel densification behavior. As defined, crystallite size refers to the size of coherent diffraction domains in XRD whereas particle size refers to the size of coherent aggregates as identified via microscopy. Therefore, a particle may consist of two or more crystallites, though given the small particle size of the presently studied materials, crystallite size and particle size are likely equivalent.

The coating work by Zu *et al*. suggests that increased size of both the particles that make up the aerogel backbone and the necks between particles also improve the robustness of the structure towards densification.[13] This hypothesis is also supported by the fact that maximum capillary pressure is inversely related to particle size. With reduced capillary pressure comes reduced driving force for densification and compaction upon heating. Molecular dynamics simulations of silica aerogel sintering also support this relationship between increasing primary particle size and reduced densification rates.[42, 43] While this mechanism remains possible, the work by Zu *et al*. does not provide data on the distribution or morphology of $SiO_2$ in relation to the $MO_x$ aerogel apart from the fact that $SiO_2$ does not crystalize up to 1000°C for $TiO_2$ and $ZrO_2$ aerogels or up to 1300°C for $Al_2O_3$ aerogels. Without distinct evidence of crystalline particles below these

temperatures, additional mechanisms must be considered. If the prevailing assumption that the $SiO_2$ coating forms the exterior of the aerogel backbone is accepted, then the surface energy is a critical parameter that has not yet been considered in the coating literature.

Reduced surface energy is hypothesized to be an important factor in improving the thermal stability of highly porous, high SSA materials such as aerogels.[3, 44] Considering the large amount of Si detected in the coated material, it can be assumed that 30YSZ-$SiO_2$ has a surface composed primary of $SiO_2$. The surface energy of amorphous silica is 0.259 J/m$^2$ if dry and 0.129 J/m$^2$ if fully hydrated.[45] This can be compared to that of 30 mol% $YO_{1.5}$-$ZrO_2$ (30YSZ), which is 0.83 J/m$^2$ if dry as averaged for a polycrystalline sample, with little dependence on whether the YSZ is crystalline or amorphous.[44] The aerogels are hydrophilic and likely have some degree of hydration on their surface, though the water adsorbed to the surface should be negligible at temperatures where sintering and densification occur. Therefore, it is sensible to compare the dry surface energies. Comparing these two values, the surface energy of amorphous $SiO_2$ (0.259 J/m$^2$) is significantly lower than that of 30YSZ (0.83 J/m$^2$). This will reduce the driving force for sintering, densification, and elimination of the surface area and associated surface energy.

As an example, one can consider the change in energy associated with surface area for a surface composed of $SiO_2$ compared to that of a surface composed of 30YSZ. Assuming a specific surface area of 400 m$^2$/g, the energy arising from the surface for $SiO_2$ is 104 J/g and for 30YSZ is 332 J/g – over a factor of three reduction in energy for $SiO_2$. In the context of a key thermodynamic driving force for sintering and densification, this reduction may prove significant. There is no evidence generated by this work to explicitly refute the previously presented hypotheses on the effect of pinning and increased particle size. Rather, the hypothesis on reduced surface energy is presented as an additional possible mechanism by which the process of coating or capping an

aerogel improves stability of the pore structure at high temperatures. Further work characterizing the starting structure of the material, namely on how the coating solution changes the YSZ aerogel's structure and chemistry, and the evolution of the $SiO_2$ in relation to the YSZ aerogel from the range of room temperature to 1000°C is required to better understand the source of thermal stability in coated metal oxide aerogels.

### 4.4 Enhanced densification beyond 1000°C with $SiO_2$ coatings

Despite a significant improvement in thermal stability with $SiO_2$ coating to 1000°C, the $SiO_2$ coating enhances densification beyond this temperature. The slope of SSA and $V_{BJH}$ in Figure 1 for coated aerogels indicate a sharp decrease in the thermal stability above 1000ºC. The SSA for 30YSZ and $SiO_2$-30YSZ are virtually identical and the mesopore volume of 30YSZ-$SiO_2$ is 2.3 times *smaller* than 30YSZ, a stark change from 1000°C, where 30YSZ-$SiO_2$ maintains 2.4 times the mesopore volume of 30YSZ. Despite the massive loss of SSA and $V_{BJH}$, the crystallite sizes of coated aerogels remain smaller than their uncoated counterparts.

Comparing the thermal stability of coated aerogels to previously studied capped and coated aerogels to temperatures of 1200°C is not possible, as Wu only measured stability to 600°C and Zu only to 1000°C for $ZrO_2$ and $TiO_2$ aerogels. It is important to note the work by Zu demonstrated that coated $Al_2O_3$ aerogels maintained good thermal stability to 1300°C with an SSA of 139 $m^2/g$. The fact that $ZrO_2$ and $TiO_2$ aerogels were reported to only 1000°C suggests these materials also densified beyond this temperature.

The TEM images of $SiO_2$-30YSZ at 1200°C in Figure 4, respectively, show a dramatic change in morphology at multiple length scales. The structure goes from a porous, web-like structure to one that appears fully dense with clearly defined spherical particles contained within a nebulous matrix. The dense appearance of the aerogel in both SEM and TEM collected after

1200°C heat treatments implies that $SiO_2$ may be flowing and enabling viscous sintering of the aerogel. Previous work has demonstrated viscous sintering is an effective means of enhancing densification and is expected to be enabled at temperatures above 1100°C for amorphous $SiO_2$.[46–49] Small particle size is expected to lower the temperature at which viscous sintering can occur in $SiO_2$, often from 50 to 100% of the bulk melting point of 1,710°C.[50–54] Structural rearrangements are also expected up to and at the glass transition temperature of 1207°C for bulk amorphous $SiO_2$ that would aid in the rearrangement and densification of the aerogel structure.[55]

The ability of $SiO_2$ to hasten densification from 1000 to 1200°C has been demonstrated in work by Fahrenholtz and Smith on diphasic aluminosilicate aerogels.[56] Diphasic aluminosilicate aerogels are composed of $Al_2O_3$-rich and $SiO_2$-rich regions. The heterogenous nature of the structure permits amorphous $SiO_2$-rich regions to persist to temperatures of 1250°C. From 1100 to 1300°C, an extraordinarily dramatic increase in density occurs for diphasic aerogels. From these previous works, it is hypothesized that viscous sintering, enabled by the presence of over 60 wt.% $SiO_2$ in SiO2-30YSZ, enhances densification, reducing the thermal stability of this material at temperatures exceeding 1000°C.

As $SiO_2$ flows, it may be filling in mesopores and aiding in the rearrangement and compaction of primary particles, leading to the dramatic reduction in mesopore volume and average mesopore size observed from 1000 to 1200°C in Figure 1. At 1200°C, there is no sign of mesoporosity in the TEM image shown in Figure 4(b), which instead reveals the formation of extremely spherical YSZ particles embedded in an amorphous $SiO_2$ matrix. The chemical compositions of these two unique areas are supported by TEM EDS data included in Figure 7(c). This effect has been reported previously for nanocrystalline YSZ polycrystals coated with a sodium strontium silicate glass.[57] Sintering at 1400°C for 1 hour led to highly faceted polyhedral

grains for uncoated YSZ and increasingly round grains for YSZ with increasing glass content. This effect was posited by the authors to be the result of the $SiO_2$ coating exerting a homogenous strain across the surface of the YSZ grains but may also result from a change in the relative surface energy of crystalline facets in YSZ. The suppression of crystallite growth of YSZ with $SiO_2$ coatings has also been previously noted and is attributed to the $SiO_2$ layers serving as grain boundary pinning agents and diffusion barriers, effectively limiting the ability of adjacent YSZ particles to diffuse together.[57, 58]

Overall, the ability of $SiO_2$ to flow at temperatures exceeding 1000°C enabled viscous sintering of the aerogel. This leads to rapid densification and destabilization of the mesoporous structure from 1000 to 1200°C. $SiO_2$-coated aerogels did not offer any improvement in thermal stability at 1200°C and will be limited to use to temperatures up to 1000°C. Despite enhancing densification of the pore structure, the $SiO_2$ coating continued to serve as a diffusion barrier, preventing the growth of crystallites to 1200°C though this is not enough to prevent destabilization of the mesoporous structure.

## 5 Summary

$SiO_2$ coated YSZ aerogels were investigated at temperatures up to 1200°C to determine pore structure stability for thermal management applications. Significant improvements in retaining the mesoporous structure of the aerogels were observed by the use of the $SiO_2$ coating up to 1000°C. The structural stability provided by the coating was largely attributed to grain boundary pinning to reduce crystallite and particle growth, in addition to reduction in surface energy, which reduces the driving force for densification. However, the amorphous $SiO_2$ coating was detrimental to pore structure stability at 1200°C due to viscous sintering. Thus, the capping/surface modification approach was moderately successful in retaining mesoporous

structure of aerogels up to 1000°C. Other coating chemistries may be considered that do not remain viscous or flow at temperatures of interest.

**Acknowledgements**

This work was supported by a NASA Space Technology Research Fellowship (80NSSC18K1189) and the NASA Aeronautics Research Mission Directorate. Characterization was carried out in part in the Materials Research Laboratory Central Research Facilities and the School of Chemical Sciences Microanalysis Laboratory, University of Illinois Urbana-Champaign (UIUC). The authors would like to thank Anita Garg from the University of Toledo for TEM analysis.

**References**

1. Hurwitz FI, Guo H, Rogers RB, *et al.* Influence of Ti addition on boehmite-derived aluminum silicate aerogels: Structure and properties. *Journal of Sol-Gel Science and Technology*. 2012;64(2):367–374. https://doi.org/10.1007/s10971-012-2866-8
2. Hurwitz FI, Rogers RB, Guo H, *et al.* Phase development and pore stability of yttria- and ytterbia-stabilized zirconia aerogels. *Journal of the American Ceramic Society*. 2020;103(12):6700–6711. https://doi.org/10.1111/jace.17376
3. Olson NS, Hurwitz FI, Guo H, *et al.* Enhanced thermal stability of high yttria concentration YSZ aerogels. *Journal of the American Ceramic Society*. 2021;104(8):4190–4202. https://doi.org/10.1111/jace.17792
4. Olson NS, Hurwitz FI, Stokes JL, Guo H, Rogers RB, Krogstad JA. Thermal stability of $M_xO_y$ -doped zirconia aerogels (M = Y, Yb, Gd, Ce, Ca) studied through 1200°C. *J Am Ceram Soc*. 2023;jace.19380. https://doi.org/10.1111/jace.19380

5. Franzel L, Wingfield C, Bertino MF, Mahadik-Khanolkar S, Leventis N. Regioselective cross-linking of silica aerogels with magnesium silicate ceramics. *Journal of Materials Chemistry A*. 2013;1(19):6021. https://doi.org/10.1039/c3ta90165c

6. Sanli D, Erkey C. Monolithic Composites of Silica Aerogels by Reactive Supercritical Deposition of Hydroxy-Terminated Poly(Dimethylsiloxane). *ACS Applied Materials & Interfaces*. 2013;5(22):11708–11717. https://doi.org/10.1021/am403200d

7. Randall JP, Meador MAB, Jana SC. Tailoring Mechanical Properties of Aerogels for Aerospace Applications. *ACS Applied Materials & Interfaces*. 2011;3(3):613–626. https://doi.org/10.1021/am200007n

8. Leventis N. Three-Dimensional Core-Shell Superstructures: Mechanically Strong Aerogels. *Accounts of Chemical Research*. 2007;40(9):874–884. https://doi.org/10.1021/ar600033s

9. Leventis N, Sotiriou-Leventis C, Zhang G, Rawashdeh AM. Nanoengineering Strong Silica Aerogels. *Nano Letters*. 2002;2(9):957–960. https://doi.org/10.1021/nl025690e

10. Mohite DP, Larimore ZJ, Lu H, Mang JT, Sotiriou-Leventis C, Leventis N. Monolithic Hierarchical Fractal Assemblies of Silica Nanoparticles Cross-Linked with Polynorbornene via ROMP: A Structure–Property Correlation from Molecular to Bulk through Nano. *Chemistry of Materials*. 2012;24(17):3434–3448. https://doi.org/10.1021/cm3017648

11. Wu NL, Wang SY, Rusakova IA. Inhibition of crystallite growth in the sol-gel synthesis of nanocrystalline metal oxides. *Science*. 1999;285(5432):1375–1377. https://doi.org/10.1126/science.285.5432.1375

12. Wang Q, Li X, Fen W, Ji H, Sun X, Xiong R. Synthesis of crack-free monolithic ZrO2 aerogel modified by SiO2. *Journal of Porous Materials*. 2014;21(2):127–130. https://doi.org/10.1007/s10934-013-9756-5

13. Zu G, Shen J, Wang W, Zhang, Z, Liu, B, Zhang, F. Robust, highly thermally stable, core-shell nanostructured metal oxide aerogels as high-temperature thermal superinsulators, adsorbents, and catalysts. *Chemistry of Materials*. 2014;26(19):5761–5772. https://doi.org/10.1021/cm502886t

14. Gash AE, Tillotson TM, Satcher JH, Hrubesh LW, Simpson RL. New sol-gel synthetic route to transition and main-group metal oxide aerogels using inorganic salt precursors. *Journal of Non-Crystalline Solids*. 2001;285(1–3):22–28. https://doi.org/10.1016/S0022-3093(01)00427-6

15. Meyer J, Olson NS, Hurwitz FI, Guo H, Stokes JL, Krogstad JA. Role of synthetic parameters on structure and thermal stability in yttria-stabilized zirconia aerogels. *Journal of Sol-Gel Science and Technology*. 2024;In press. DOI: 10.1007/s10971-023-06292-7.

16. Scherer GW. Theory of Drying. *Journal of the American Ceramic Society*. 1990;73(1):3–14. https://doi.org/10.1111/j.1151-2916.1990.tb05082.x

17. Garvie RC. The occurrence of metastable tetragonal zirconia as a crystallite size effect. *Journal of Physical Chemistry*. 1965;69(4):1238–1243. https://doi.org/10.1021/j100888a024

18. Garvie RC. Stabilization of the tetragonal structure in zirconia microcrystals. *Journal of Physical Chemistry*. 1978;82(2):218–224. https://doi.org/10.1021/j100491a016

19. Kwon SY, Kim W-Y, Hudon P, Jung I-H. Thermodynamic modeling of the CaO-$SiO_2$-$ZrO_2$ system coupled with key phase diagram experiments. *Journal of the European Ceramic Society*. 2017;37(3):1095–1104. https://doi.org/10.1016/j.jeurceramsoc.2016.10.011

20. Zhang F, Chen M, Zhang S, Zhou P, Du Y. Thermodynamic modeling of $ZrO_2$–$Y_2O3$–$SiO_2$ and $ZrO_2$-$Gd_2O_3$–$SiO_2$ systems. *Calphad*. 2021;72:102248. https://doi.org/10.1016/j.calphad.2020.102248

21. Shashidhara PS, Thomas JK. Phase relations in the system CaO-$SiO_2$-$ZrO_2$. *Steel Research*. 1994;65(10):410–413.

22. Wagstaff FE. Crystallization and Melting Kinetics of Cristobalite. *Journal of the American Ceramic Society*. 1969;52(12):650–654. https://doi.org/10.1111/j.1151-2916.1969.tb16069.x

23. Wagstaff FE. Crystallization Kinetics of Internally Nucleated Vitreous Silica. *Journal of the American Ceramic Society*. 1968;51(8):449–453. https://doi.org/10.1111/j.1151-2916.1968.tb11917.x

24. Wagstaff FE, Richards KJ. Kinetics of Crystallization of Stoichiometric $SiO_2$ Glass in $H_2O$ Atmospheres. *Journal of the American Ceramic Society*. 1966;49(3):118–121. https://doi.org/10.1111/j.1151-2916.1966.tb15387.x

25. Breneman RC, Halloran JW. Kinetics of Cristobalite Formation in Sintered Silica. *Journal of the American Ceramic Society*. 2014;97(7):2272–2278. https://doi.org/10.1111/jace.12889

26. Li X, Yin X, Zhang L, He S. The devitrification kinetics of silica powder heat-treated in different conditions. *Journal of Non-Crystalline Solids*. 2008;354(28):3254–3259. https://doi.org/10.1016/j.jnoncrysol.2008.02.016

27. Al-Hasnawi AAK, Al-Hydary IAD. The devitrification kinetics of transparent silica glass prepared by gel-casting method. *Matéria (Rio de Janeiro)*. 2019;24(1). https://doi.org/10.1590/s1517-707620190001.0654

28. Wu NL, Wang SY, Rusakova IA. Inhibition of crystallite growth in the sol-gel synthesis of nanocrystalline metal oxides. *Science*. 1999;285(5432):1375–1377. https://doi.org/10.1126/science.285.5432.1375

29. Castro RHR, Gouvêa D. Sintering and Nanostability: The Thermodynamic Perspective. *Journal of the American Ceramic Society*. 2016;99(4):1105–1121. https://doi.org/10.1111/jace.14176

30. Nafsin N, Aguiar JA, Aoki T, Thron AM, van Benthem K, Castro RHR. Thermodynamics versus kinetics of grain growth control in nanocrystalline zirconia. *Acta Materialia*. 2017;136:224–234. https://doi.org/10.1016/j.actamat.2017.07.005

31. Li H, Dey S, Castro RHR. Kinetics and thermodynamics of densification and grain growth: Insights from lanthanum doped zirconia. *Acta Materialia*. 2018;150:394–402. https://doi.org/10.1016/j.actamat.2018.03.033

32. Castro RHR. On the thermodynamic stability of nanocrystalline ceramics. *Materials Letters*. 2013;96:45–56. https://doi.org/10.1016/j.matlet.2013.01.007

33. Shi JL, Lin ZX, Yen TS. Effect of dopants on the crystallite growth of superfine zirconia powder. *Journal of the European Ceramic Society*. 1991;8(2):117–122. https://doi.org/10.1016/0955-2219(91)90117-I

34. Shi JL, Ruan ML, Yen TS. Crystallite growth in yttria-doped superfine zirconia powders and their compacts: A comparison between Y-TZP and YSZ. *Ceramics International*. 1996;22(2):137–142. https://doi.org/10.1016/0272-8842(95)00069-0

35. Matsui K, Yoshida H, Ikuhara Y. Grain-boundary structure and microstructure development mechanism in 2-8 mol% yttria-stabilized zirconia polycrystals. *Acta Materialia*. 2008;56(6):1315–1325. https://doi.org/10.1016/j.actamat.2007.11.026

36. Chen IW. Mobility control of ceramic grain boundaries and interfaces. *Materials Science and Engineering A*. 1993;166(1–2):51–58. https://doi.org/10.1016/0921-5093(93)90309-3

37. Wang X, Chen I. Sintering dense nanocrystalline ceramics without final-stage grain growth. *Nature*. 2000;404(9 March):168–171.

38. Hwang S -L, Chen I -W. Grain Size Control of Tetragonal Zirconia Polycrystals Using the Space Charge Concept. *Journal of the American Ceramic Society*. 1990;73(11):3269–3277. https://doi.org/10.1111/j.1151-2916.1990.tb06449.x

39. Lange FF. Transformation-Toughened ZrO2: Correlations between Grain Size Control and Composition in the System ZrO2-Y2O3. *Journal of the American Ceramic Society*. 1986;69(3):240–242. https://doi.org/10.1111/j.1151-2916.1986.tb07416.x

40. De Souza DPF, De Souza MF. Liquid Phase Sintering of RE2O3: YSZ Ceramics Part I Grain Growth and Expelling of the Grain Boundary Glass Phase. *Journal of Materials Science*. 1999;34:4023–4030.

41. Clarke DR. On the Equilibrium Thickness of Intergranular Glass Phases in Ceramic Materials. *Journal of the American Ceramic Society*. 1987;70(1):15–22. https://doi.org/10.1111/j.1151-2916.1987.tb04846.x

42. Brinker CJ, Scherer GW. Sol-Gel Science. Elsevier; 1990 https://doi.org/10.1016/C2009-0-22386-5

43. Yang MY, Tang GH, Sheng Q, Guo L, Zhang H. Atomic-level sintering mechanism of silica aerogels at high temperatures: structure evolution and solid thermal conductivity. *International Journal of Heat and Mass Transfer*. 2022;199:123456. https://doi.org/10.1016/j.ijheatmasstransfer.2022.123456

44. Drazin JW, Castro RHR. Phase stability in nanocrystals: A predictive diagram for yttria-zirconia. *Journal of the American Ceramic Society*. 2015;98(4):1377–1384. https://doi.org/10.1111/jace.13504

45. Brunauer S, Kantro DL, Weise CH. The surface energies of amorphous silica and hydrous amorphous silica. *Canadian Journal of Chemistry*. 1956;34(10):1483–1496. https://doi.org/10.1139/v56-190

46. Scherer GW. Viscous Sintering of Particle Filled Composites. *American Ceramic Society Bulletin*. 1991;70:1059–1063.

47. Zhuravlev LT. The surface chemistry of amorphous silica. Zhuravlev model. *Colloids and Surfaces A: Physicochemical and Engineering Aspects*. 2000;173(1–3):1–38. https://doi.org/10.1016/S0927-7757(00)00556-2

48. Ivankovic H, Tkalcec E, Nass R, Schmidt H. Correlation of the precursor type with densification behavior and microstructure of sintered mullite ceramics. *Journal of the European Ceramic Society*. 2003;23(2):283–292. https://doi.org/10.1016/S0955-2219(02)00176-0

49. Sacks MD, Bozkurt N, Scheiffele GW. Fabrication of Mullite and Mullite-Matrix Composites by Transient Viscous Sintering of Composite Powders. *Journal of the American Ceramic Society*. 1991;74(10):2428–2437. https://doi.org/10.1111/j.1151-2916.1991.tb06780.x

50. Kobata A, Kusakabe K, Morooka S. Growth and transformation of $TiO_2$ crystallites in aerosol reactor. *AIChE Journal*. 1991;37(3):347–359. https://doi.org/10.1002/aic.690370305

51. Xiong Y, Pratsinis SE. Formation of agglomerate particles by coagulation and sintering-Part I. A two-dimensional solution of the population balance equation. *Journal of Aerosol Science*. 1993;24(3):283–300. https://doi.org/10.1016/0021-8502(93)90003-R

52. Xiong Y, Kamal Akhtar M, Pratsinis SE. Formation of agglomerate particles by coagulation and sintering—Part II. The evolution of the morphology of aerosol-made titania, silica and silica-doped titania powders. *Journal of Aerosol Science*. 1993;24(3):301–313. https://doi.org/10.1016/0021-8502(93)90004-S

53. Seto T, Hirota A, Fujimoto T, Shimada M, Okuyama K. Sintering of polydisperse nanometer-sized agglomerates. *Aerosol Science and Technology*. 1997;27(3):422–438. https://doi.org/10.1080/02786829708965482

54. Tsantilis S, Pratsinis SE, Briesen H. Sintering Time for Silica Particle Growth. *Aerosol Science and Technology*. 2001;34(3):237–246. https://doi.org/10.1080/02786820119149

55. Ojovan MI, Tournier RF. On structural rearrangements near the glass transition temperature in amorphous silica. *Materials*. 2021;14(18):1–16. https://doi.org/10.3390/ma14185235

56. Fahrenholtz WG, Smith DM, III JC. Effect of Precursor Particle Size on the Densification and Crystallization Behavior of Mullite. *Journal of the American Ceramic Society*. 1993;76(2):433–437. https://doi.org/10.1111/j.1151-2916.1993.tb03802.x

57. Ramamoorthy R, Chaim R. Microstructural evolution in nanocrystalline Y-TZP containing a silicate glass. *Journal of the European Ceramic Society*. 2001;21(16):2895–2902. https://doi.org/10.1016/S0955-2219(01)00215-1

58. Aguilar DH, Torres-Gonzalez LC, Torres-Martinez LM, Lopez T, Quintana P. A Study of the Crystallization of ZrO2 in the Sol–Gel System: $ZrO_2$–$SiO_2$. *Journal of Solid State Chemistry*. 2001;158(2):349–357. https://doi.org/10.1006/jssc.2001.9126